ARGONNE NATIONAL LABORATORY
9700 South Cass Avenue, Argonne, Illinois 60439

DART Model for Thermal Conductivity of U_3Si_2 Aluminum Dispersion Fuel

J. Rest, J. L. Snelgrove, and G. L. Hofman

September 1995

Presented at the 18th International
Meeting on Reduced Enrichment for Research
and Test Reactors, 18-21 September, 1995,
Paris, France

DART Model for Thermal Conductivity of U_3Si_2 Aluminum Dispersion Fuel

by

J. Rest, J. L. Snelgrove, and G. L. Hofman

Abstract

This paper describes the primary physical models that form the basis of the DART model for calculating irradiation-induced changes in the thermal conductivity of aluminum dispersion fuel. DART calculations of fuel swelling, pore closure, and thermal conductivity are compared with measured values.

1 Introduction

DART [1], a thermomechanical model for the prediction of fission-product-induced swelling in aluminum dispersion fuels, has been applied to the analysis of U_3Si and U_3Si_2 dispersion fuel swelling in plate, tube, and rod fuel element geometries for research reactor applications. The model calculates irradiation-induced swelling of fission gas bubbles as a function of fuel morphology. The DART mechanical model calculates the behavior of a rod, tube, or plate during closure of as-fabricated porosity, during which the fuel particle swelling is accommodated by the relatively soft aluminum matrix flowing into the existing porosity; it also calculates the subsequent macroscopic changes in rod diameter or plate/tube thickness caused by additional fuel deformation processes. DART also includes a calculation for the effect of irradiation on the thermal conductivity of the dispersion fuel, and for fuel restructuring due to the aluminum fuel reaction, amorphization, and recrystallization. This paper describes the primary physical models that form the basis of the DART model for calculating irradiation-induced changes in the thermal conductivity of dispersion fuel.

2 DART Model for Irradiation-Induced Changes in Thermal Conductivity of Dispersion Fuel

The DART thermal conductivity model accounts for the dependence of thermal conductivity on both as–fabricated and irradiation-induced porosity. For dispersion fuels, two distinct classes of pores exist: fission gas microbubbles generated within the U_3Si_2 fuel particles,and as–fabricated voids contained within the aluminum matrix. Where pore geometry and physical properties are of prime importance, the analytical treatment of such pores is, however, similar. Pore geometry is defined by its size, shape, and orientation with respect to the direction of heat flow. Physical properties of importance are the emissivity of the pore surface and the thermal conductivity of the gas trapped within the pore. Figure 1 can be used to establish a geometric relationship for the thermal conductivity of a solid material containing a gas pore. The unit cell can be represented as a cube of solid material surrounding a spherical pore. The most important variable considered, and the one that appears in all theoretical models [2-4], is the volume porosity P, defined as

$$P = \frac{\text{Pore Volume}}{\text{Pore Volume + Volume of Solid}}. \quad (1)$$

If we assume that heat flows in the y direction only, the effective thermal conductivity k_e of the unit cell in the y direction is given by

$$k_e = P_c k_{ap} + (1 - P_c) k_s, \quad (2)$$

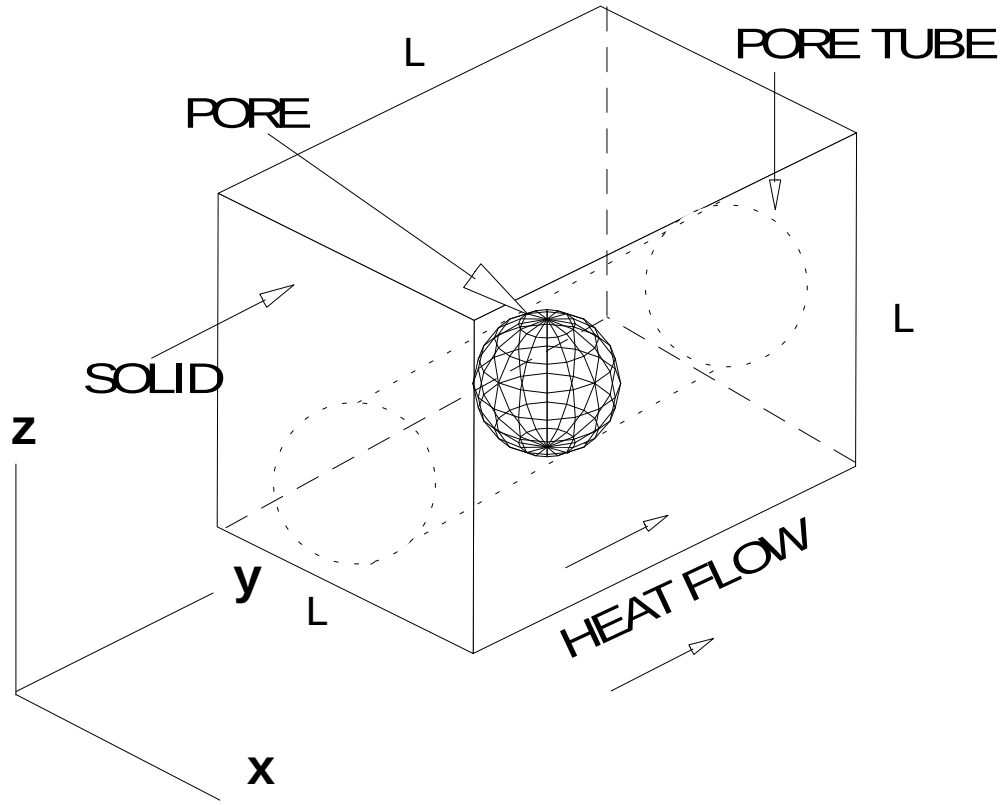

Fig. 1. Representation of unit cell of a porous body for which effective thermal conductivity is assessed.

where k_g = effective thermal conductivity, k_s = thermal conductivity of solid material, k_{ap} = apparent thermal conductivity of the pore tube, and P_c is the fraction of the cross–sectional area of the x–z face of the unit cell that is occupied by the pore. To assess the conductance over the path length in the y direction, we define a pore tube length L that considers both the pore and the solid material that occupies the remaining tube length. The apparent thermal conductance of the pore tube (pore plus solid material in the path length) can be evaluated by considering the thermal resistance of these two regions; it can be expressed as

$$\frac{1}{k_{ap}} = \frac{P_L}{k_p} + \frac{1 - P_L}{k_s}, \tag{3}$$

where P_L = fractional length of pore and k_p = effective pore thermal (gas conductivity plus radiation). By eliminating k_{ap} between Eqs. 2 and 3, we obtain the following expression [5,6]:

$$\frac{k_e}{k_s} = 1 - P_c\left(1 - \frac{k_p / k_s}{P_L}\right). \tag{4}$$

In Eq. 4, the effect of volume porosity on thermal conductance is contained in the quantities P_c and P_L. For the case of fission gas bubbles within U_3Si_2 fuel particles, it is assumed that the bubbles are spherical, with a radius R_g, and are uniformly spaced in the material. Under these assumptions, the following expressions apply:

$$P_c = \pi R_g^2 / l_g^2 = \pi \phi^2 R_g^2 \left(\rho_g\right)^{2/3}, \tag{5}$$

$$P_L = 2R_g / l_g = 2\phi R_g \left(\rho_g\right)^{1/3}, \tag{6}$$

where ρ_g is the bubble density (bubbles/cc), l_g is the interbubble spacing, and ϕ is a geometric factor that relates the average interbubble spacing to the bubble density, i.e., $l_g = \phi \rho_g^{-1/3}$. For uniformly spaced gas bubbles, $\phi = 1.25$.

The thermal conductivity of a pore filled with gas is given by [7]

$$k_p = k_g + 4\varepsilon\sigma R T^3, \tag{7}$$

where k_g = bulk thermal conductivity of the gas, ε = emissivity, σ = Stefan–Boltzmann constant, and T = temperature.

For the size pores and range of temperatures under consideration, the second term in Eq. 7, representing radiative heat transfer, can be neglected. Thus, Eq. 4, when applied to gas bubbles, reduces to the form

$$k_e^g / k_f = 1 - \left[\pi R_g^2 \left(\rho_g\right)^{2/3}\right]\left[1 - k_g / \left(2k_f R_g \rho_g^{1/3}\right)\right], \tag{8}$$

where k_e^g = effective thermal conductivity of fuel particles that contain fission gas, and k_f = thermal conductivity of bulk U_3Si_2.

Equation 8 can be written in the form

$$k_e^g / k_f = 1 - \pi\left(R_g / l_g\right)^2 + \frac{\pi k_g}{2k_f}\left(R_g / l_g\right), \tag{9}$$

where the ratio of the bubble radius R_g to interbubble spacing l_g can be expressed as $R_g / l_g = \phi^{-1} R_g \rho_g^{1/3} = \phi^{-1} \sum_\alpha \sum_i R_i^\alpha \left(C_i^\alpha\right)^{1/3}$, where C_i^α is the number of α -type bubbles in the i-th size

class per unit volume with radius R_i^{α} ; $\alpha = 1,2,3,4$ represents the lattice, dislocation, grain face, and grain edge distributions, respectively, and i sums over the bubble size distribution.

The geometric condition for bubble interconnection is given by $l_g = 2R_g$. Equations 8 and 9 represent expressions for k_e^g / k_f in terms of average properties of the fission gas bubble size distribution that evolves within the U_3Si_2 fuel particles during irradiation. The expression for k_g that is used to evaluate Eqs. 8 and 9, as given in Ref. 4, is

$$k_g(\text{xenon}) = \left(4.0288\text{x}10^5\right) T^{0.872} \ (\text{W / mK}). \tag{10}$$

To include the effects of both as–fabricated and irradiation-induced porosity on the thermal conductivity of U_3Si_2 particles dispersed in an aluminum matrix, successive applications of a mixing formula of the form given by Eq. 9 have been utilized. For example, the thermal conductivity of aluminum containing a dispersion of U_3Si_2 particles (i.e., containing fission gas) with no as–fabricated porosity is given by

$$k_e^p = 1 - \left(\pi R_f^2 \rho_f{}^{2/3}\right)\left[1 - k_e^g / \left(2k_{al} R_f \rho_f{}^{1/3}\right)\right], \tag{11}$$

where k_e^p = effective thermal conductivity of dispersion with no as–fabricated porosity, R_f = radius of particle, k_e^g = effective thermal conductivity of U_3Si_2 particles containing fission gas (given by Eq. 9), ρ_f = density of U_3Si_2 particles, and k_{al} = thermal conductivity of pure aluminum.

If as–fabricated porosity is now introduced into the material,

$$\frac{k_e^m}{k_e^p} = 1 - \pi R_p^2 \rho_p^{2/3}, \tag{12}$$

where k_e^m = thermal conductivity of dispersion, containing both as–fabricated and irradiation-induced porosity; R_p °= radius of as–fabricated pores; and ρ_p = density of as–fabricated porosity.

In deriving Eq. 12, the thermal conductivity of an as–fabricated pore has been assumed to be zero. For particles dispersed in aluminum and for the distribution of as-fabricated porosity, ϕ = 1. Utilizing Eqs. 11 and 12, we can express k_e^m as

$$\begin{aligned} k_e^m = k_{al}\Big[&Z_1 + Z_2 F_f^{2/3} + Z_3\left(k_e^g / k_{al}\right) F_f^{1/3}\left(1 + Z_2 F_p{}^{2/3}\right) \\ &+ Z_2 F_p^{2/3} + Z_4\left(F_f F_p\right)^{2/3}\Big], \end{aligned} \tag{13}$$

where the fuel and pore volume fractions F_f and F_p are given by

$$F_f = \frac{4}{3}\pi R_f^3 \rho_f , \tag{14}$$

$$F_p = \frac{4}{3}\pi R_p^3 \rho_p , \tag{15}$$

and where Z_1 - Z_4 are constants:

$$\begin{aligned} Z_1 &= 1 \\ Z_2 &= -\pi(3/4\pi)^{2/3} = -1.208993 \\ Z_3 &= (\pi/2)(3/4\pi)^{1/3} = 0.974442 \\ Z_4 &= \pi^2(3/4\pi)^{4/3} = 1.461666 \end{aligned} \tag{16}$$

Implicit in the derivation of Eq. 13 is the assumption of a homogeneous distribution of spherical particles (i.e., fission gas, as–fabricated pores, U_3Si_2 particles) within the respective host materials, such as is characteristic of extruded rods. To quantify the effects of deviations from this idealized geometry, such as nonspherical pores and particles characteristic of rolled plates, and as–fabricated and irradiation-induced pores preferentially distributed along the particle/matrix interface (e.g., fission gas released from the grain interior can collect at the particle/matrix interface), the constant Z_4 was determined by regression analysis, based on unirradiated dispersion fuel data from Ref. 8, shown in Table 1 to be:

$$Z_4 = 0.6521 . \tag{17}$$

Equation 13 is valid as long as the matrix aluminum is the continuous media. An analogous expression to Eq. 13 can be derived for cases where the fuel is the continuous media, and is given by

$$\begin{aligned} k_e^m = k_e^g \Big[& Z_1 + Z_2 F_{al}^{2/3} + Z_3 \left(k_{al} / k_e^g\right) F_{al}^{1/3} \left(1 + Z_2 F_p{}^{2/3}\right) \\ & + Z_2 F_p^{2/3} + Z_4' \left(F_{al} F_p\right)^{2/3} \Big], \end{aligned} \tag{18}$$

where F_{al} is the aluminum volume fraction. In Eq. 18, Z_4' can be determined by requiring that Eqs. 13 and 18 yield the same result at a critical fuel and pore volume fraction (data for cases where the fuel is the continuous media are not currently available).

In Eq. 17, Z_4 has been determined based on comparison with plate-fuel conductivity measurements in the transverse (thickness) direction. As such, Eq. 13 with Z_4 given by Eq. 17 is valid for thermal conductivity

calculations in the transverse direction only. An extension of Eq. 13 to conductivity calculations in the longitudinal direction can be obtained by an appropriate utilization of measured anisotropy in U_3Si_2 ground-powder-based fuel plates [9]

The results of the analysis are shown in Table 1 and Figs. 2 and 3. Figure 2 shows the results of the regression analysis performed with Eq. 13 and with the data listed in Table 1. Figure 3 shows the thermal conductivity data and the results calculated for thermal conductivity with Eqs. 13 and 17, plotted against the volume fraction of fuel plus voids. Also shown in Figs 2 and 3 are calculations using Eqs. 13 and 16 compared with U_3Si dispersion fuel data from extruded rods [10]. Because of the manner in which this fuel has been fabricated, the pore and particle shapes are close to spherical. The reasonable agreement between Eqs. 13 and 16 and the extruded-rod data shown in Figs. 2 and 3 provide support for the physical basis of Eq. 13. Figure 4 shows the DART–calculated thermal conductivity for U_3Si fuel as a function of irradiation–induced porosity, and measured values [11] for irradiated and subsequently annealed bulk U_3Si. The effect of swelling porosity on the thermal conductivity of irradiated U_3Si was deduced from electrical conductivity measurements on samples with pore volume fractions of 0.01-0.27. The authors of Ref. 11 state that the porosity in the irradiated and annealed U_3Si consists of fission gas as compared with predominantly empty voids in the irradiated-only case. As shown in Fig. 4, the DART-calculated change in thermal conductivity agrees reasonably well with the measured values.

Equations 13 and 18 provide physically based expressions for the evolution of thermal conductivity in irradiated dispersion fuels. As such, even though the geometric constant Z_4 was determined from unirradiated data, Eqs. 13 and 18 embody physically realistic functional dependencies, e.g., the dependence of thermal conductivity on fuel and matrix volume fractions and on as–fabricated and irradiation-induced porosity, which allow for a reasonable extrapolation to irradiated materials.

Because calculation of the irradiation behavior of the thermal conductivity in dispersion fuels depends critically on the calculated fuel swelling and pore closure, validation of the DART swelling models is examined in the next section prior to the presentation of the DART thermal conductivity calculations in Section 4.

3 DART Validation for Irradiation Behavior of Various Designs of Uranium Silicide Dispersion Fuel Elements

The DART mechanical (stress) model consists of a fuel sphere that deforms because of swelling due to both solid fission products and fission gas bubbles. The fuel sphere is surrounded by an aluminum matrix shell, which is assumed to behave in a perfectly plastic manner and which deforms (yields) when fuel particle volume expands. The effects of cladding are included by a suitable adjustment of the effective aluminum volume fraction. Currently, the effects of creep are not included; instead, the stress relaxation is approximated by lowering the aluminum yield stress to an “effective” value. Different values of this effective yield stress

Table 1. Results of regression analysis from Eq. 13, and data from Ref. 8

#	k_e^m (W/mK)	F_f (%)	F_p (%)	k_e^g / k_{al}	k_e^m / k_{al}	
					Data	Model
01	70.9	32.5	6.9	0.06607	0.31652	0.3122
02	75.5	34.0	6.9	0.06607	0.33705	0.2969
03	33.0	39.7	10.5	0.06607	0.14732	0.1908
04	34.0	38.4	11.6	0.06607	0.15179	0.1890
05	39.0	38.0	12.4	0.06607	0.17411	0.1828
06	12.0	49.9	18.4	0.06607	0.05357	0.0121
07	181.0	13.7	1.9	0.06607	0.80804	0.6353
08	78.0	32.3	6.0	0.06607	0.34821	0.3286
09	40.0	39.4	9.2	0.06607	0.17857	0.2108
10	48.0	37.0	9.3	0.06607	0.21429	0.2325
11	40.0	39.1	9.5	0.06607	0.17857	0.2097
12	59.0	46.4	4.0	0.06607	0.26339	0.2225
13	59.0	46.4	4.0	0.06607	0.26339	0.2225
14	13.9	46.4	15.4	0.06607	0.06205	0.0729
15	14.5	46.9	15.4	0.06607	0.06473	0.0686

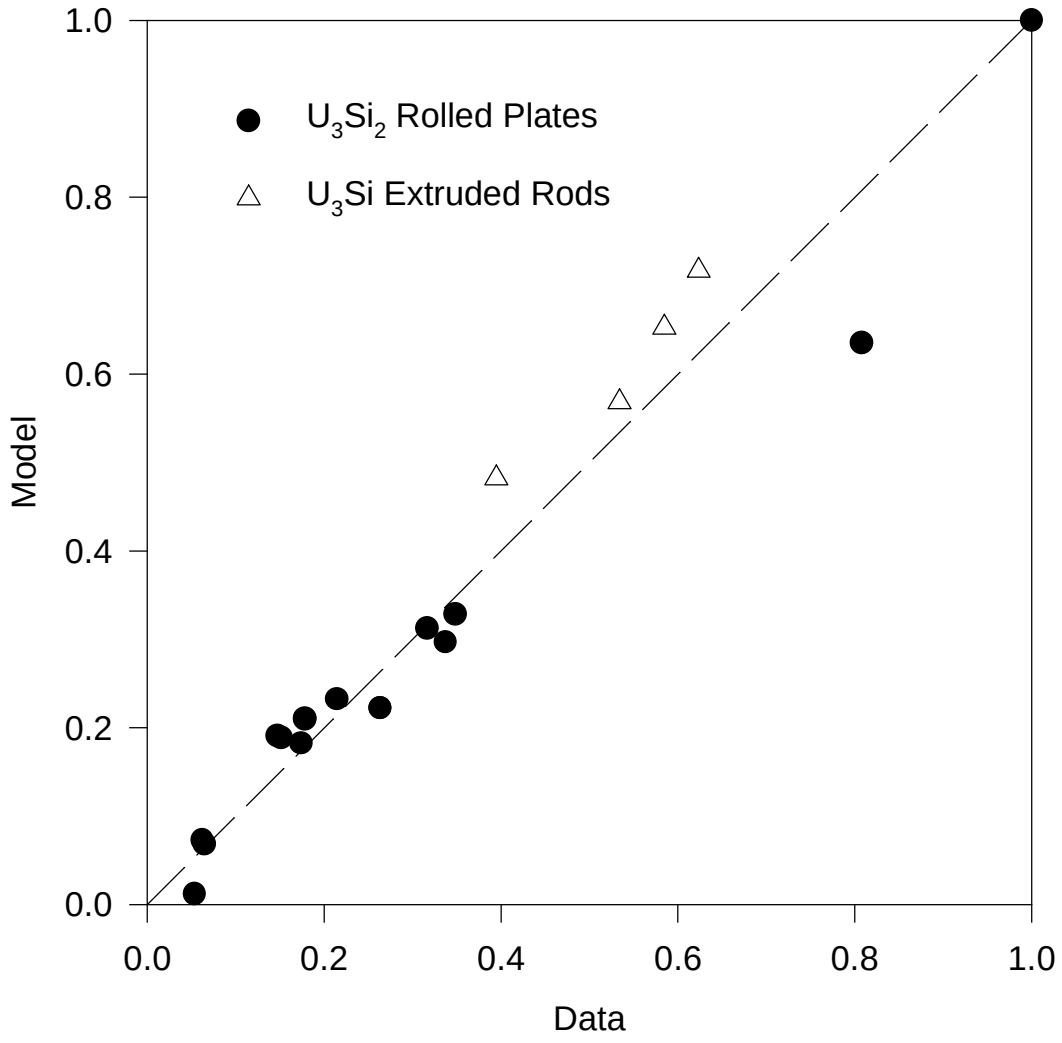

Fig. 2. Results of regression analysis obtained from Eq. 13 and from data in Table 1. Also shown are calculations using Eqs. 13 and 16 compared with data from Ref. 10.

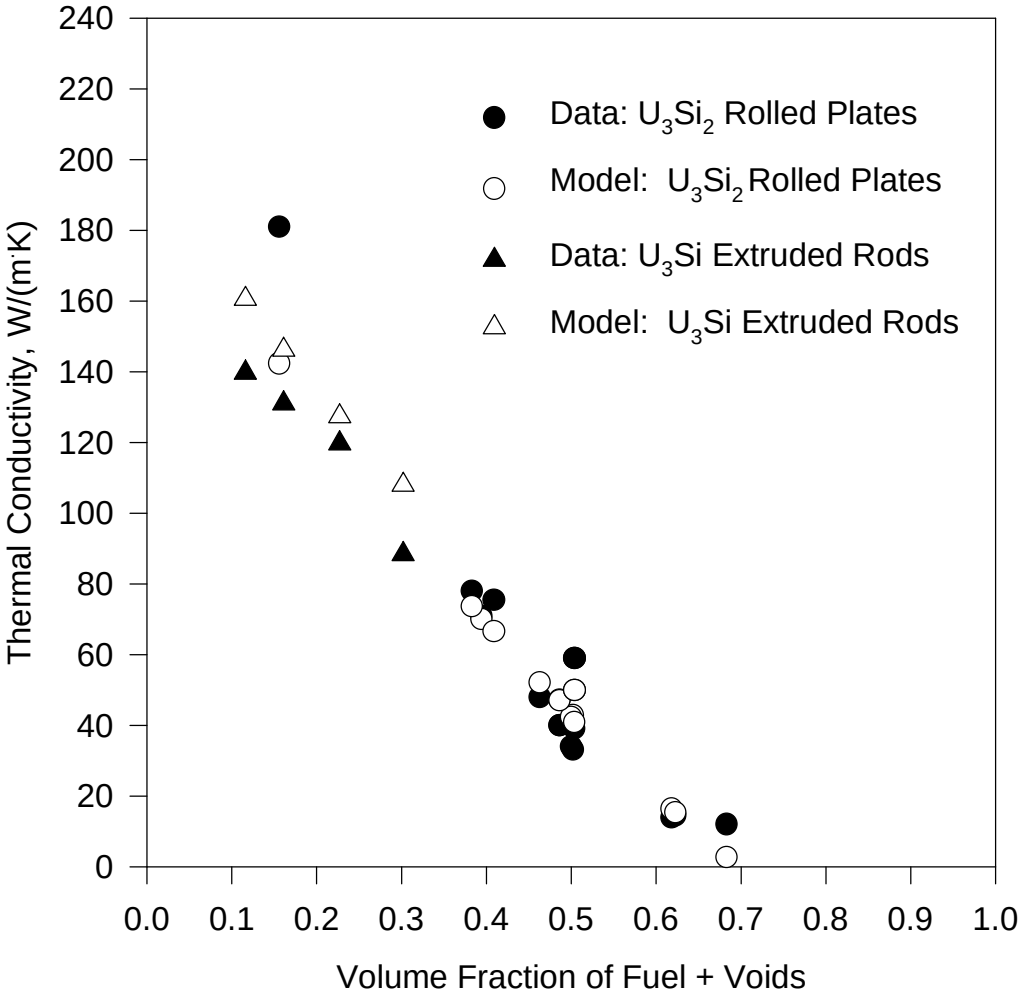

Fig. 3. Thermal conductivity obtained from Eq. 13 and from data listed in Table 1, as a function of volume fraction of fuel + voids. Also shown are calculations using Eqs. 13 and 16 compared with data from Ref. 10.

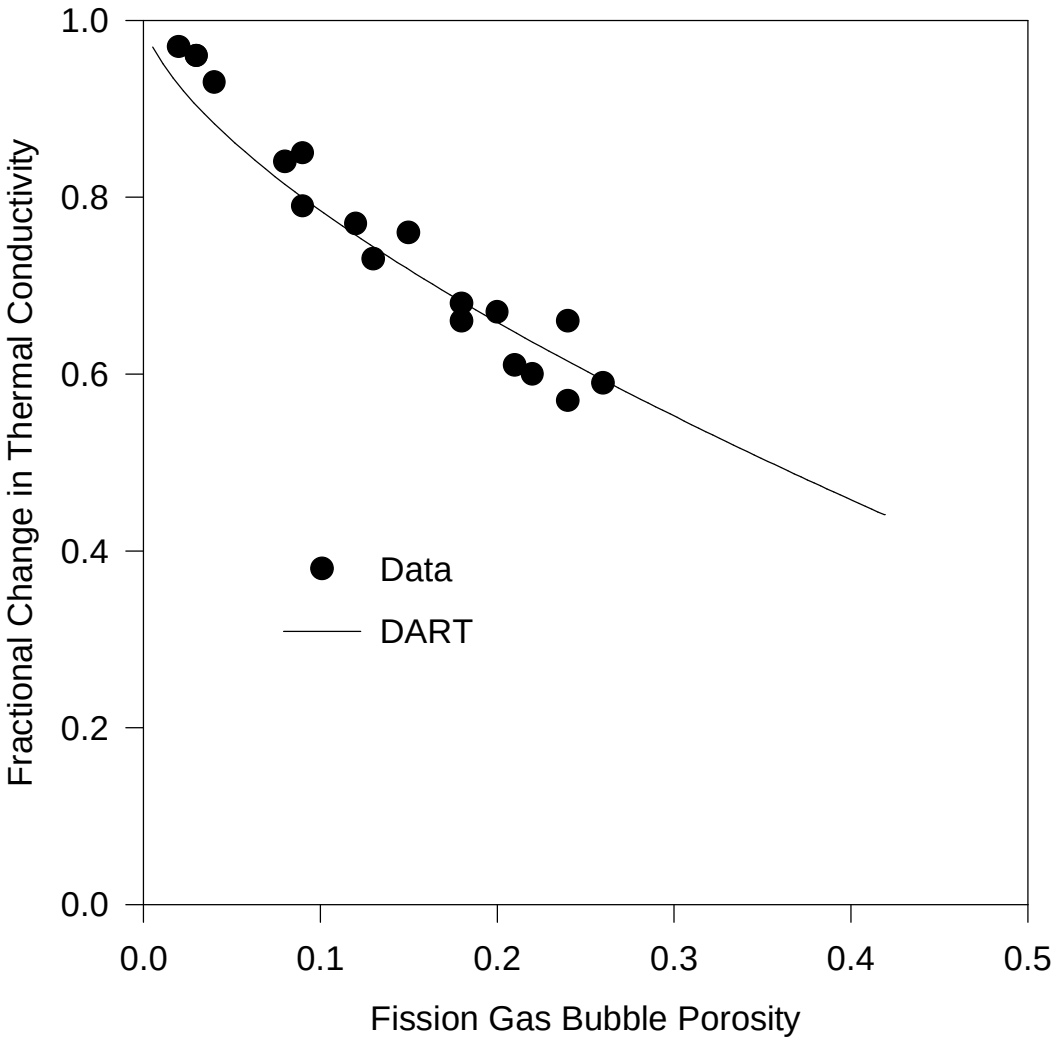

Fig. 4. DART-calculated and measured (deduced from electrical conductivity measurements) change in thermal conductivity for U_3Si fuel as a function of irradiation-induced porosity in irradiated and subsequently annealed bulk U_3Si

are used for the rod, plate, and tube geometries to simulate the quite complicated time-dependent deformation behavior of the rod and plate with the rather simplistic DART stress model. The deformation of the matrix and cladding material generates stresses within the expanding fuel particles, which affect the swelling rate of the fission gas bubbles. The swelling fuel particles push the matrix aluminum into as-fabricated porosity and simultaneously cause cladding deformation. The swelling rate primarily depends on the plastic yielding of the aluminum matrix and cladding. The hydrostatic stress σ_i (i = 1,2 refers to plate or rod geometry), acting on the gas bubbles is given by

$$\sigma_i = \frac{2}{3}\left[1 - \ln\left(\frac{V_o^F + \Delta V^F}{V_o^C}\right)\beta_i \sigma_{Al}^Y(T)\right], \tag{19}$$

where $\sigma_{Al}^Y(T)$ is the as-fabricated temperature-dependent yield strength of the aluminum, $\frac{V_o^F + \Delta V^F}{V_o^C}$ is the fuel volume fraction, and β_i is a factor that accounts for the effects of irradiation (e.g., irradiation-enhanced creep). The values of β_i used in DART are $\beta_1 = 7.5$ and $\beta_2 = 2.5$.

Results of DART calculations are shown in Figs. 5 and 6. The calculations shown in Figs. 5 and 6 were all performed at the same constant fuel temperature of 373 K. Figure 5 shows DART results for fuel swelling of U_3SiAl-Al in plate, tube, and rod configurations as a function of fission density compared with data. The lower calculated fuel swelling in the rod-type element is due to an assumed biaxial stress state rather than to an assumed uniaxial stress state for the plate and thin-walled tube geometries. Fuel swelling in plates results in plate thickness increase only, while plate width and length remain relatively unchanged. Likewise, in tubes, only the wall thickness increases and the overall diameter remains unchanged. Thus, cladding of these element designs contains minimal lateral or circumferential strain and consequently, much less restraint compared with the hoop stress state in a solid-clad rod. Irradiation experiments have shown that plate-type dispersion fuel elements can develop blisters or pillows at high ^{235}U burnup when fuel compounds exhibiting breakaway swelling, such as U_3SiAl and U_3Si, are used at moderate to high fuel volume fractions. The U_3SiAl plate data shown in Fig. 5 exhibits this behavior at fission densities above about $\approx 5 \times 10^{27}$ m^{-3}. Figure 6 shows DART-calculated results for fuel particle swelling of low-enriched U_3Si_2-Al fuel plates and rods as a function of fission density. The calculated values shown in Fig. 6 indicate that irradiation-induced recrystallization occurred at $\approx 3.5 \times 10^{27}$ m^{-3}. Again, the fuel rods exhibit lower values of swelling than the plates because of the greater restraint imposed by the rod configuration.

Figure 7 shows DART-calculated results for pore closure of low-enriched U_3Si_2 fuel plates fabricated to 50% and 13% fuel and pore volume fractions, respectively, compared with the measured values. The DART calculations show the effects of fuel recrystallization (increased rate of pore closure), which is calculated to occur at a fission density of 3.5×10^{27} m^{-3}. As is evident from Figs. 5-7 , DART-calculated fuel swelling and pore closure are in reasonable agreement with observation.

4 DART Calculation of Dispersion Fuel Thermal Conductivity

Figures 8 and 9 show the results of DART calculations of the bulk thermal conductivity and total fuel swelling, respectively, of a 3.5-g/cm^3 35% enriched U_3Si_2 dispersion fuel containing 3.5% as-fabricated porosity for four values of fuel temperature. The calculations shown in Figs. 8 and 9 utilized a one-node mesh across the fuel plate, and a 20-node mesh across the fuel particle.

Each thermal conductivity curve shown in Fig. 8 exhibits a characteristic shape: initially, the thermal conductivity increases because of pore closure in response to fuel particle swelling; this is followed by a decrease in the thermal conductivity due to additional fuel particle swelling and a commensurate decrease in the volume fraction of aluminum; subsequently, an accelerated decrease in the thermal conductivity occurs because of the onset of grain subdivision, which leads to higher fuel particle swelling rates (see Fig. 9). Two predictions of the temperature dependence of the thermal conductivity are shown in Fig. 8. First, for the initial phase of the irradiation that includes pore closure (up to the onset of grain subdivision), lower thermal conductivities are predicted for the irradiations at higher temperatures because of aluminide formation. Aluminide formation is faster at higher temperatures and results in an increase in fuel swelling (see Fig. 9) because the density of the aluminide is reduced beyond that of the original U_3Si_2 . Second, for a constant fission rate, grain subdivision is predicted to occur earlier for irradiations at higher temperatures. As the swelling rate increases upon grain subdivision (see Fig. 9), the thermal conductivity starts an accelerated decrease earlier at the higher temperatures. This behavior is shown more clearly in Fig. 10, where the DART-calculated bulk thermal conductivity and total fuel swelling of a 1.3-g/cm^3, 92.5% enriched U_3Si_2 dispersion fuel containing 0.7% as-fabricated porosity are exhibited. Increased fission rates (enrichments) result in higher thermal conductivity predictions (all other conditions remaining constant) because of the delay in the onset of grain subdivision. The calculations shown in Fig. 10 were performed at a constant fuel temperature of 373 K and utilized a one-node mesh across the fuel plate and a 20-node mesh across the fuel particle.

As described above, the thermal conductivity curve shown in Fig. 10 exhibits a characteristic shape: initially, the thermal conductivity increases as pore closure occurs; this is followed by a decrease in the thermal conductivity due to fuel particle swelling, an accelerated decrease in the thermal conductivity due to the onset of grain subdivision(grain refinement leads to higher fuel swelling rates); and, finally, at high burnup, we observe an additional accelerated decrease in the thermal conductivity due to the transformation of the interior of the fuel particles to an unstable phase [1].

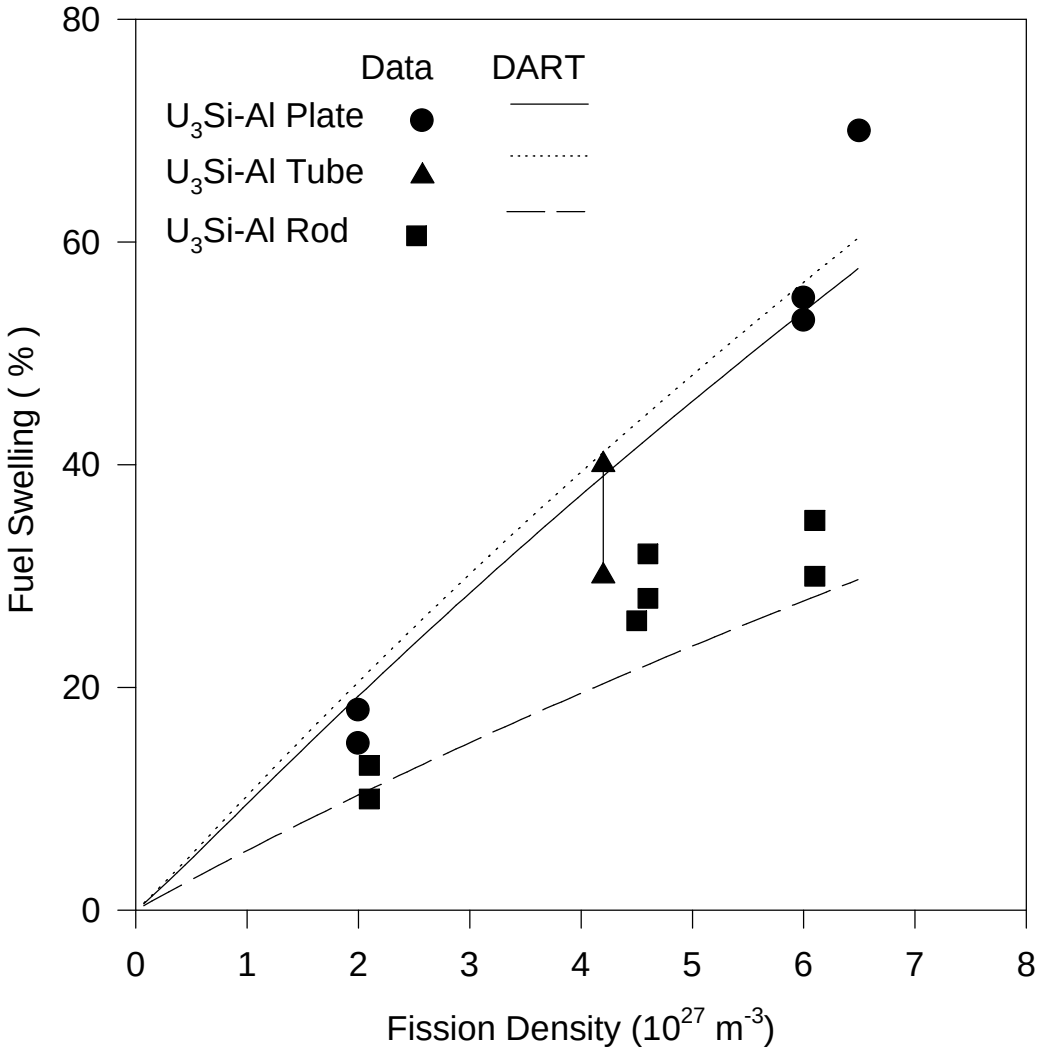

Fig. 5. DART results for swelling of U_3SiAl-Al in plate, tube, and rod configurations as a function of fission density compared with data

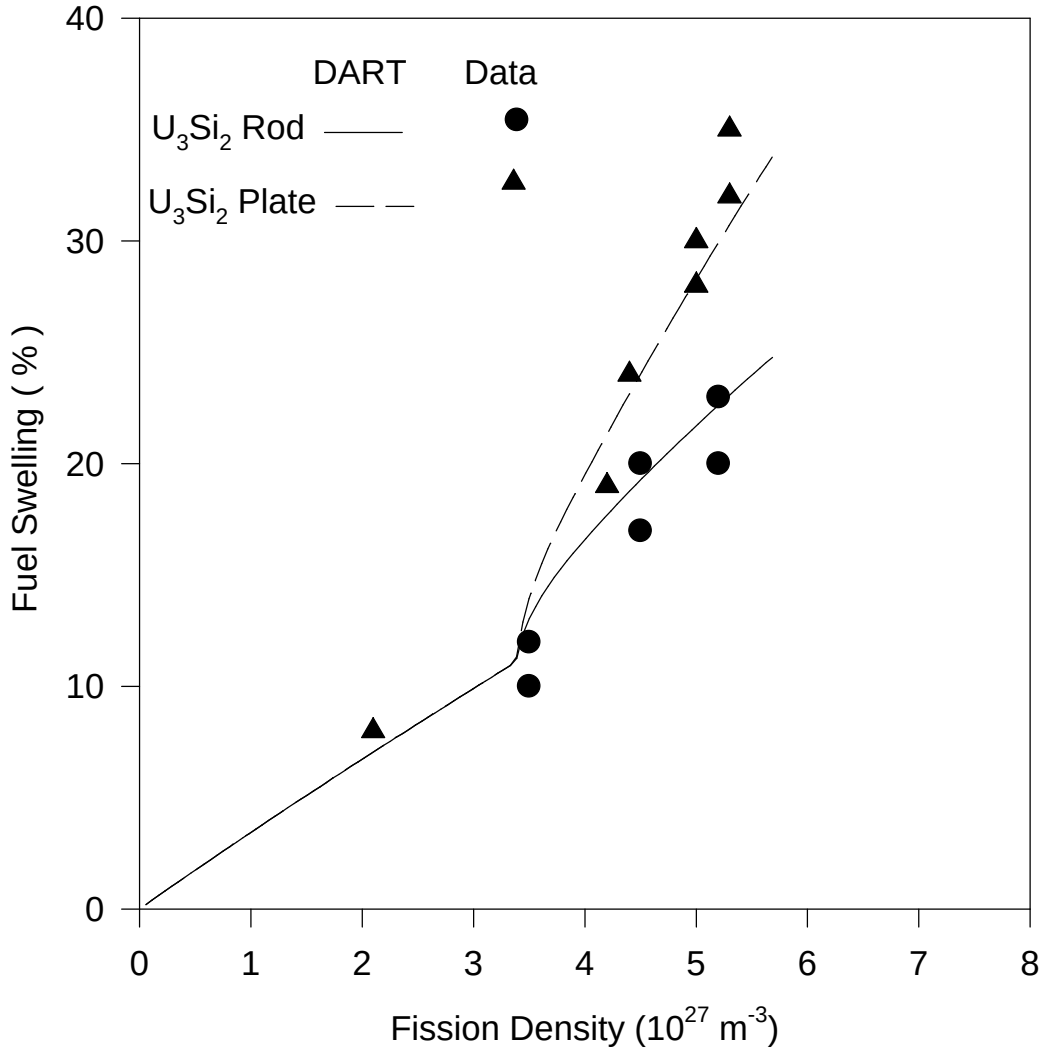

Fig. 6. DART-calculated results for fuel particle swelling of low-enriched U_3Si_2-Al fuel plates and rods as a function of fission density

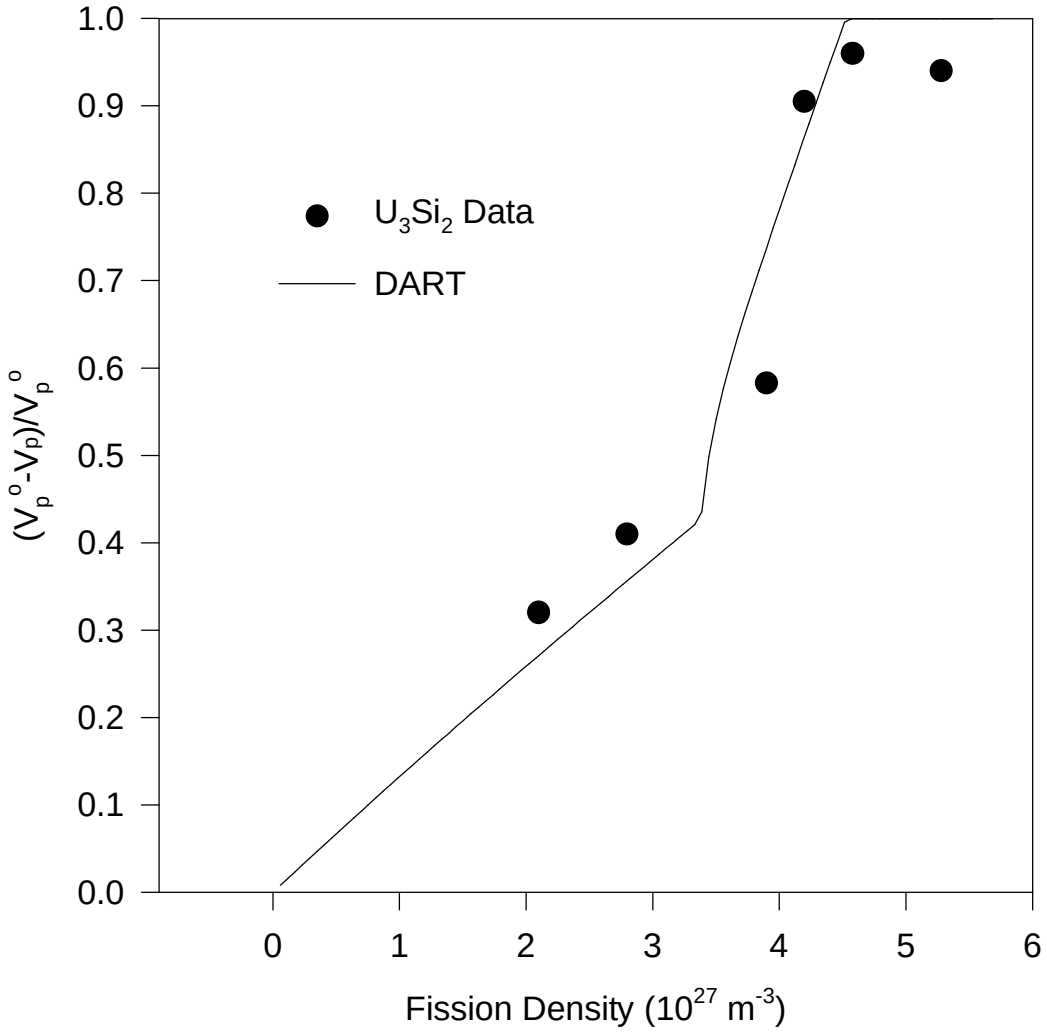

Fig. 7. DART-calculated results for pore closure of low-enriched U_3Si_2 fuel plates as a function of fission density compared with the measured values

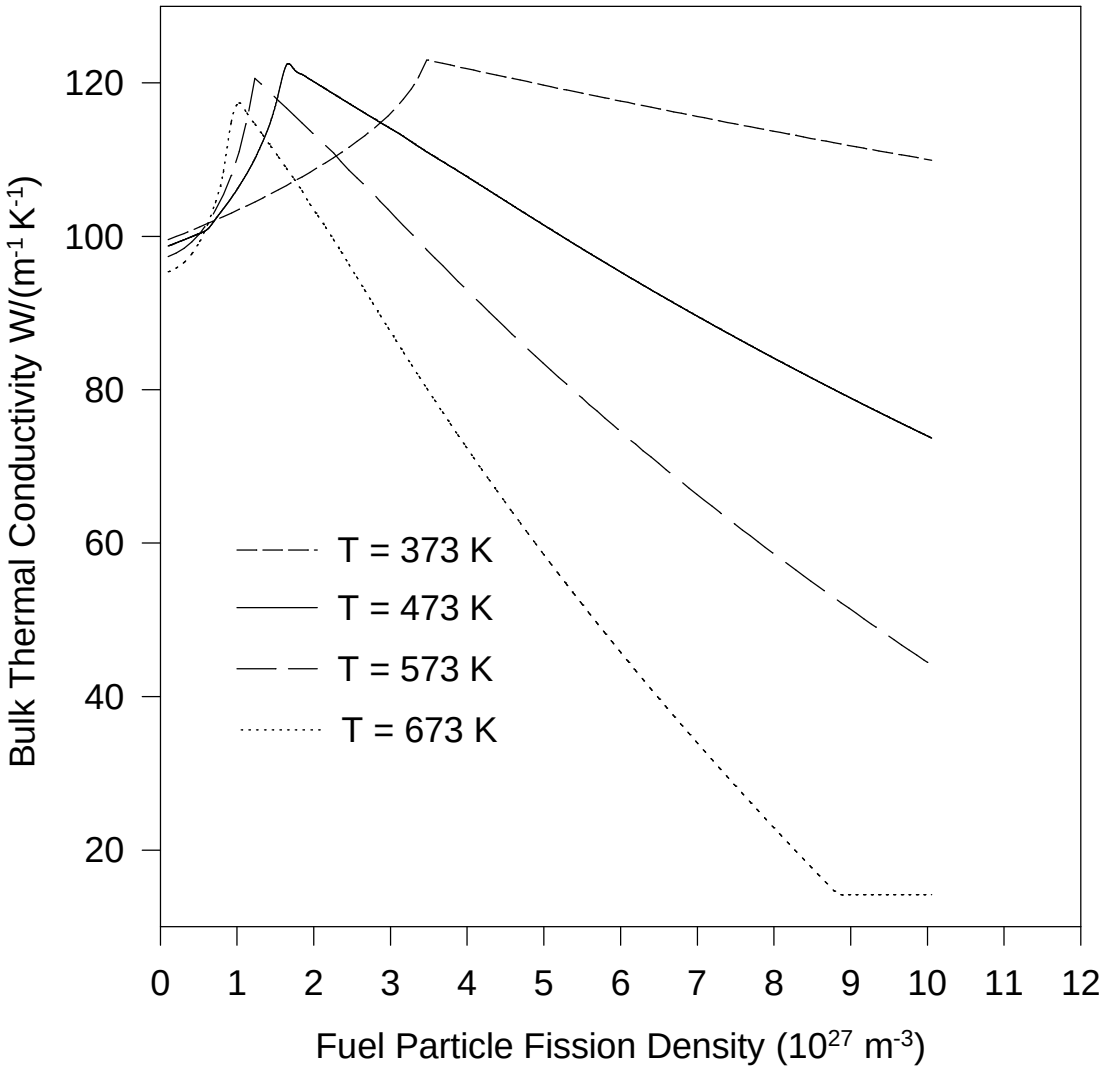

Fig. 8. DART calculated bulk thermal conductivity of a 3.5-g/cm^3, 35% enriched U_3Si_2 dispersion fuel containing 3.5% as-fabricated porosity, at four fuel temperatures

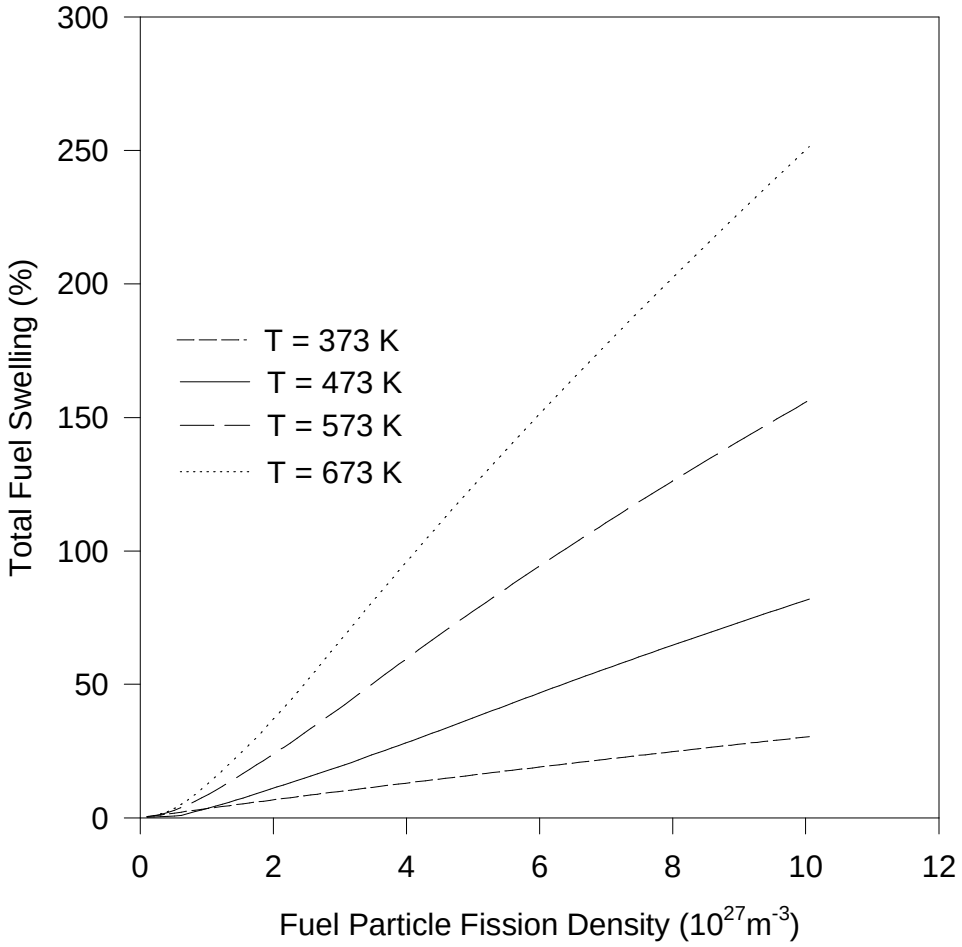

Fig. 9. DART calculated total fuel swelling (%) of a 3.5-g/cm^3, 35% enriched U_3Si_2 dispersion fuel containing 3.5% as-fabricated porosity, at four fuel temperatures

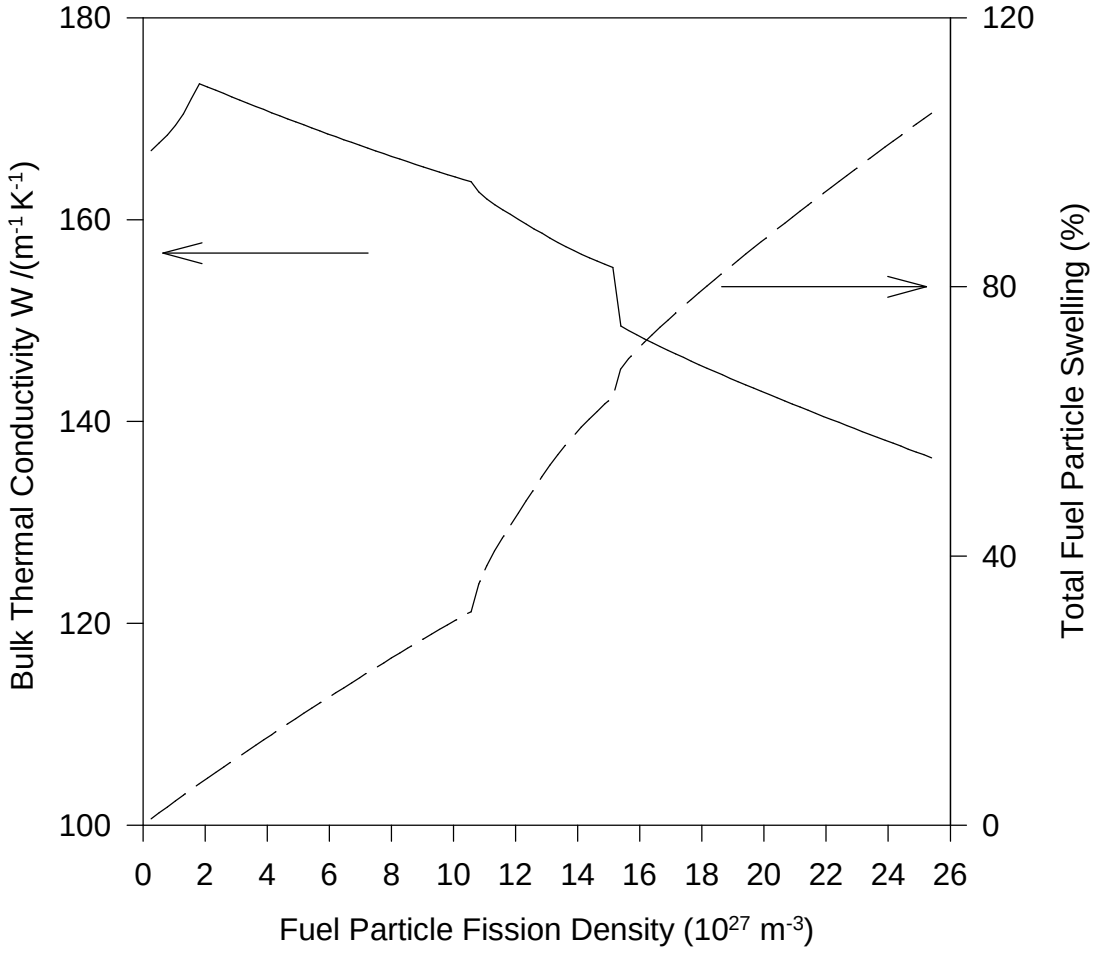

Fig. 10. DART-calculated bulk thermal conductivity and total fuel swelling of a 1.3-g/cm^3, 92.5% enriched U_3Si_2 dispersion fuel containing 0.7% as-fabricated porosity, irradiated at 373 K

References

1. J. Rest, *The DART Dispersion Analysis Research Tool: A Mechanistic Model for the Prediction of Fission-Product Induced Swelling of Aluminum Dispersion Fuels,* Argonne National Laboratory Report ANL-95/36 (1995).

2 . M. Jakob, *Heat Transfer*, John Wiley and Sons, London (1969), pp. 83-88.

3 . W. H. McAdams, *Heat Transmission*, McGraw-Hill, New York (1954), p. 10, 1954.

4 . D. R. Olander, *Fundamental Aspects of Nuclear Reactor Fuel Elements*, U.S. Dept. of Energy Publication, TID–26711–P1, (1976).

5 . A. L. Loeb, *Thermal Conductivity: VIII, A Theory of Thermal Conductivity of Porous Materials*, J. Am. Ceram. Soc. **37**, 96 (1954).

6 . H. Kampf and G. Karsten, *Effects of Different Types of Void Volumes as the Radial Temperature Distribution of Fuel Pins*, J. Nucl. Technol. **9**, 288 (1970).

7 . G. A. Reymann and D. L. Hagrmann, *MATRPO–10: A Handbook of Material Properties for Use in the Analysis of LWR Fuel Rod Behavior*, TREE–NUREG–1180, EG&G–Idaho, Inc. Report, 1978.

8 . R. K. Williams,.R. S. Graves, R. F. Domagala, and T. C. Wiencek, *Thermal Conductivities of U_3Si and U_3Si_2-Al DISPERSION FUELS*, in Thermal Conductivity, **19**, Plenum Publishing Corp. (1988), p. 271.

9. C. K. Kim, C. T. Lee, H. D. Park, K. H. Kim, and I. H. Kuk, *The Effect of Particle Shape on Thermal and Electrical Conductivities of Uranium Silicide Dispersion Fuel*, in Proc. 16th Intl. Meeting on Reduced Enrichment for Research and Test Reactors, Oarai, Japan, March 1994.

10. W. S. Ryu, Y. H. Kang, K. N. Choo, J. M. Park, C. T. Lee, and I. H. Kuk, *Physical Properties of Atomized U_3Si-Al Fuel Meat,* in Proc. 16th Intl. Meeting on Reduced Enrichment for Research and Test Reactors, Oarai, Japan, March 1994.

11. I. J. Hastings, J. R. MacEwan, and L. R. Bourque, *Effect of Swelling on Thermal Conductivity and Postirradiation Densification of U_3Si*, J. Amer. Ceram. Soc., **55** (5), 240 (1972).